Chinese Chemical Letters 36 (2025) 110258

Contents lists available at ScienceDirect

Chinese Chemical Letters

journal homepage: www.elsevier.com/locate/cclet

FRET-based *in vitro* assay for rapid detecting of SARS-CoV-2 entry inhibitors

Chunyu Yan[a,b], Qinglong Qiao[a], Wei Zhou[a], Xuelian Zhou[a,b], Yonghui Chen[a], Lu Miao[a,*], Zhaochao Xu[a,b,*]

[a] Dalian Institute of Chemical Physics, Chinese Academy of Sciences, Dalian 116023, China
[b] School of Chemistry, Dalian University of Technology, Dalian 116024, China

ARTICLE INFO

Article history:
Received 7 June 2024
Revised 12 July 2024
Accepted 15 July 2024
Available online 15 July 2024

Keywords:
SARS-CoV-2
FRET
RBD-ACE2 interaction
Inhibitor
Fluorescence detection
Protein labeling

ABSTRACT

The continuous mutation and rapid spread of the severe acute respiratory syndrome coronavirus 2 (SARS-CoV-2) have led to the ineffectiveness of many antiviral drugs targeting the original strain. To keep pace with the virus' evolutionary speed, there is a crucial need for the development of rapid, cost-effective, and efficient inhibitor screening methods. In this study, we created a novel approach based on fluorescence resonance energy transfer (FRET) technology for *in vitro* detection of inhibitors targeting the interaction between the SARS-CoV-2 spike protein RBD (s-RBD) and the virus receptor angiotensin-converting enzyme 2 (ACE2). Utilizing crystallographic insights into the s-RBD/ACE2 interaction, we modified ACE2 by fusing SNAP tag to its N-terminus (resulting in SA740) and Halo tag to s-RBD's C-terminus (producing R525H and R541H), thereby ensuring the proximity (<10 nm) of labeled FRET dyes. We found that relative to the R541H fusion protein, R525H exhibited higher FRET efficiency, which attributed to the shortened distance between FRET dyes due to the truncation of s-RBD. Utilizing the sensitive FRET effect between SA740 and R525H, we evaluated its efficacy in detecting inhibitors of SARS-CoV-2 entry in solution and live cells. Ultimately, this FRET-based detection method was demonstrated high sensitivity, rapidity, and simplicity in solution and held promise for high-throughput screening of SARS-CoV-2 inhibitors.

The development of antiviral drugs targeting the treatment of severe acute respiratory syndrome coronavirus 2 (SARS-CoV-2) remains an urgent need to respond to the current coronavirus disease 19 (COVID-19) pandemic, as the virus continues to mutate and spread relentlessly. Widely studied druggable targets include virus-encoded structural proteins (*e.g.*, spike glycoprotein and nucleocapsid protein), proteases and RNA polymerases, as well as host-based targets such as angiotensin-converting enzyme 2 (ACE2) receptor, transmembrane serine protease 2 (TMPRSS2), and cathepsin l. One promising therapeutic approach is to target the interaction between the receptor binding domain (RBD) of the SARS-CoV-2 spike protein and the host cell ACE2. This strategy aims to effectively hinder viral entry since the robust binding between RBD and ACE2 constitutes the initial stage of viral infection [1,2]. By high-throughput drug screening, inhibitors targeting the RBD-ACE2 binding (RAB) have been identified, including selective antibodies against the spike protein RBD (s-RBD), antibodies binding to ACE2 (although these antibodies may have side effects), and small molecules that directly bind to either RBD or ACE2 [3-6]. Despite these efforts, most RAB inhibitors become ineffective as the virus continues to mutate under natural selection [7-9]. Developing rapid and effective methods for inhibitor screening can swiftly identify inhibitors for new viral variants, to adapt to the evolved forms of the virus.

The *in vitro* screening methods are widely used for the preliminary screening of drugs due to their rapidity, low cost, and high throughput [10-12]. Various screening methods for RAB inhibitors have been developed. For instance, in the early stages of the COVID-19 pandemic, researchers conducted high-throughput screening of potential therapeutic drugs targeting RAB using virtual screening and molecular docking techniques [13-16]. However, computer simulations, usually grounded in existing data and assumptions, may not encompass all biological activities and drug properties, potentially resulting in substantial screening inaccuracies [17,18]. The enzyme-linked immunosorbent assay (ELISA) is another widely employed method for screening RAB inhibitors. However, it involved multiple steps including coating antigen, sequential addition of blocking agent, sample, substrate, as well as washing between each step, thus requiring a longer time to obtain results.

* Corresponding authors.
E-mail addresses: miaolu@dicp.ac.cn (L. Miao), zcxu@dicp.ac.cn (Z. Xu).

https://doi.org/10.1016/j.cclet.2024.110258
1001-8417/

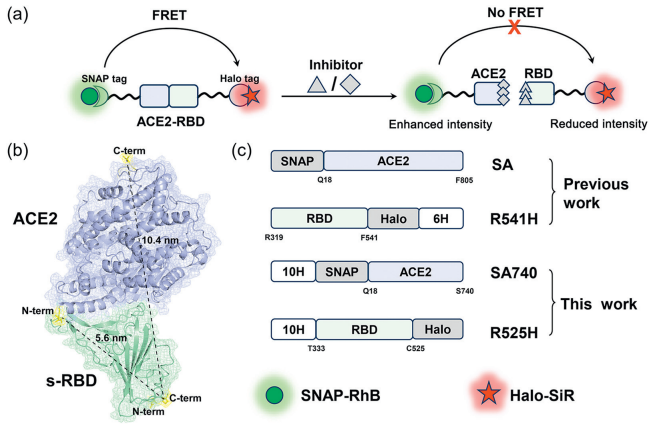

Scheme 1. Assay design for FRET based RAB inhibitors screening *in vitro*. (a) Schematic representation of the inhibitor screening strategy: SNAP-dye and Halo-dye FRET pairs were labeled to SARS-CoV-2 s-RBD and ACE2, allowing us to monitor RAB by tracking the FRET signal between the dyes in solution. s-RBD/ACE2 inhibitors can block RAB, resulting in a decrease in FRET signal, thereby facilitating the detection of RAB inhibitors. (b) Crystal structure of SARS-CoV-2 s-RBD complexed with ACE2 soluble part, PDB ID: 6VW1. (c) Schematic representation of plasmid constructs and SNAP/Halo FRET dyes most used in this paper.

Fluorescence detection offers high sensitivity, simplicity, and rapidity. Techniques based on fluorescence resonance energy transfer (FRET) have been employed in the screening of numerous proteins for drug discovery [19-21]. Gorshkov's group labeled RBD with inorganic quantum dots (QDs) to mimic virus infection and screen inhibitors according to the energy transfer between QDs and Au nanoparticles. But the non-quantitative protein labeling (one QD connected with multiple s-RBDs) and single signal response greatly reduced the accuracy of drug efficacy evaluation, which limited their further application [22]. Das *et al.* used fluorescent proteins to study the specific process of Rac1 signal polarization through FRET, but the lower fluorescence intensity and photostability of them are limited for fluorescence recognition [23]. Small molecule fluorophores stand out due to their remarkable photophysical properties and biocompatibility [24-27]. Protein tags such as SNAP-tag and Halo-tag enable the covalent attachment of small molecule dyes to the protein of interest *in situ*, facilitating real-time monitoring of protein-protein interactions and widely employed in live-cell. In our previous work, we utilized genetically encoded SNAP/Halo protein tag to label dyes to s-RBD and ACE2 protein for live-cell rapid drug screening and the study of viral infection mechanisms [28,29]. A small molecule inhibitor targeting RAB was screened out.

In this paper, we labeled the s-RBD and ACE2 soluble proteins with FRET dyes, allowing us to monitor RAB in real time by tracking the FRET signal between the dyes in solution. This enabled the development of a rapid screening method for inhibitors of the ACE2-RBD interaction (Scheme 1). Expanding on previous work, Halo and SNAP tags were fused to soluble proteins s-RBD and ACE2. Through detecting various FRET dye pairs and s-RBD fragment lengths, we identified SNAP-ACE2-dye and Halo-RBD-dye complex proteins capable of producing significant FRET effects. These complexes enable the rapid detection of RBD-neutralizing antibodies, S protein, small molecule inhibitors, and other RAB inhibitors in solution. This approach holds promise for high-throughput screening of RAB inhibitors *in vitro*.

To achieve efficient FRET, several conditions must be met. Firstly, the emission spectrum of the donor fluorophore should overlap with the absorption spectrum of the acceptor fluorophore. Furthermore, the donor fluorophore should have a high quantum yield, while the acceptor fluorophore possesses a favorable extinction coefficient. Importantly, the distance between the donor and acceptor molecules should be within 10 nm to facilitate effective energy transfer. By analyzing the crystal structure of the interaction between s-RBD and the soluble portion of ACE2 (Scheme 1b, PDB ID: 6VW1), it was revealed that the C-terminus of s-RBD is proximal to its N-terminus and distanced from the region where it interacts with ACE2. The distances between the C-terminus/N-terminus of ACE2 and the C-terminus of s-RBD were determined to be 10.4 and 5.6 nm, respectively. Hence, to ensure that the distance of dye pairs labeling to s-RBD and ACE2 are within 10 nm after the binding of s-RBD to ACE2 protein, protein tags must exclusively be fused to the N-terminus of the ACE2 protein. In our earlier work, we fused SNAP to the N-terminus of the full sequence of ACE2 (residues Q18-F805) to create the SA fusion protein, while the Halo tag was fused to the C-terminus of s-RBD to obtain RBD (319–541)-Halo (R541H) (Scheme 1c). Live-cell fluorescence imaging confirmed the stable interaction between SA and R541H [28]. Here, to optimize the proximity of the FRET dye pair after the binding of s-RBD and ACE2 protein, we fused the SNAP tag to the N-terminus of the soluble portion of ACE2 (Q18-S740), resulting in SNAP-ACE2 (Q18-S740) (SA740). Additionally, we truncated the s-RBD segment to further shorten the distance between the dye pairs, obtaining RBD (333–525)-Halo (R525H) (Scheme 1c). Meanwhile, a His tag was added to these fusion proteins for protein purification purposes.

We obtained SA740, R525H, and R541H fusion protein through mammalian cell expression and Ni-NTA purification. The relatively singular protein bands observed in sodium dodecyl sulfate-polyacrylamide gel electrophoresis (SDS-PAGE) indicated the purity of these fusion proteins (Fig. S1 in Supporting information). The molecular weight of R525H and R541H fusion proteins is approximately 59 kDa, while that of SA740 is approximately 120 kDa. The small molecule fluorescent dye TMSiR exhibits excellent properties, such as membrane permeability, near-infrared emission, high photostability, and signal-to-noise ratio, making it widely applied in super-resolution imaging techniques like stimulated emission depletion (STED) [30,31]. The significant spectral overlap between SNAP-600/SNAP-RhB emission spectrum and TMSiR absorption spectrum, along with the high molar extinction coefficient of TMSiR, led to its selection as the FRET acceptor in this study. Therefore, for FRET-based RAB detection *in vitro*, two donor-acceptor dyes pairs, SNAP-600/Halo-SiR and SNAP-RhB/Halo-SiR, and a group of non-FRET dyes SNAP-Alexa488/Halo-SiR were selected to label SA740 and R525H fusion protein, respectively. The absorption and emission spectra of the three dye pairs were shown in Figs. 1b-d. Upon exposure to ultraviolet light in a darkroom, distinct fluorescent bands can be observed on the SDS-PAGE gel of SA740-SNAP-RhB, R525H–Halo-SiR, and R541H–Halo-SiR (Fig. 1a). These fluorescent bands correspond to the positions of the protein bands stained with Coomassie brilliant blue, indicating that the three proteins fused with SNAP/Halo tags can be specifically and covalently labeled with fluorescent dyes. Benefiting from the SNAP/Halo protein self-labeling technology, a variety of organic dyes with SNAP/Halo substrates can be labeled to s-RBD/ACE2.

To detect the FRET effect after the interaction between s-RBD and ACE2 in solution, we mixed SA740-dye and R525H-dye in equal proportions. And then the fluorescence spectra of SA740-dye, R525H-dye, and the mixed solution were measured separately by exciting the donor dye wavelength. Their fluorescence emission spectra revealed that, under excitation of donor excitation wavelength at 560 and 520 nm, respectively, both their acceptor R525H-SiR could emit the fluorescence of TMSiR, corresponding to a decrease in donor fluorescence intensity and an increase in acceptor fluorescence, indicating the effective of FRET between s-RBD and ACE2 (Figs. 1e and f). On the contrary, there was no FRET for the protein labeled with SNAP-Alexa488/Halo-SiR dyes (Fig. 1g).

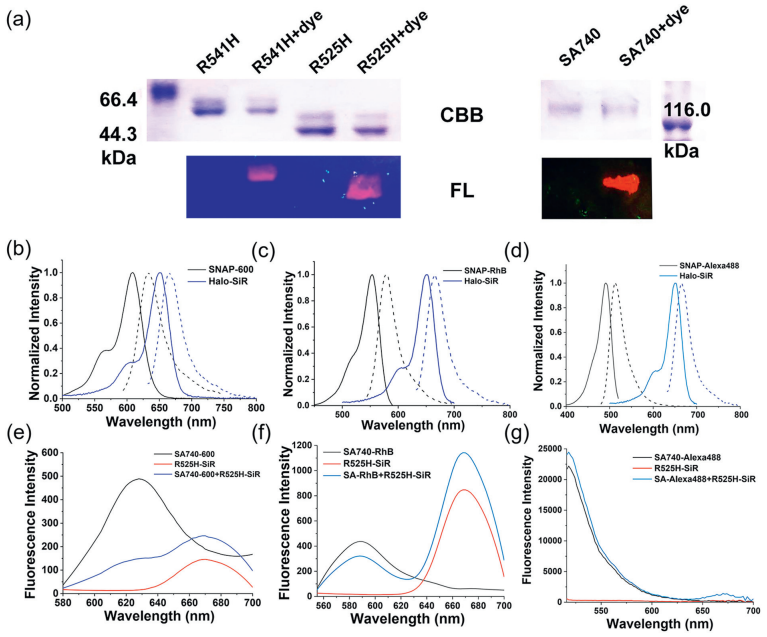

Fig. 1. SDS-PAGE and Spectra analysis of RAB *in vitro*. (a) SDS-PAGE of the fusion protein R525H, R541H, and SA740 before and after labeling with dyes Halo-SiR and SNAP-600. (b-d) The normalized absorbance (solid lines) and fluorescence (spot lines) spectra of SNAP-600/Halo-SiR (b), SNAP-RhB/Halo-SiR (c), and SNAP-Alexa488/Halo-SiR (d) pairs. (e–g) fluorescence spectra of SA740-dye and R525H-dye interaction after being labeled with (b-d) donor-acceptor pairs. The concentration of each protein-dye sample was 0.5 μmol/L. $\lambda_{ex} = 540/520$ nm for (e) and (f), $\lambda_{ex} = 488$ nm for (g).

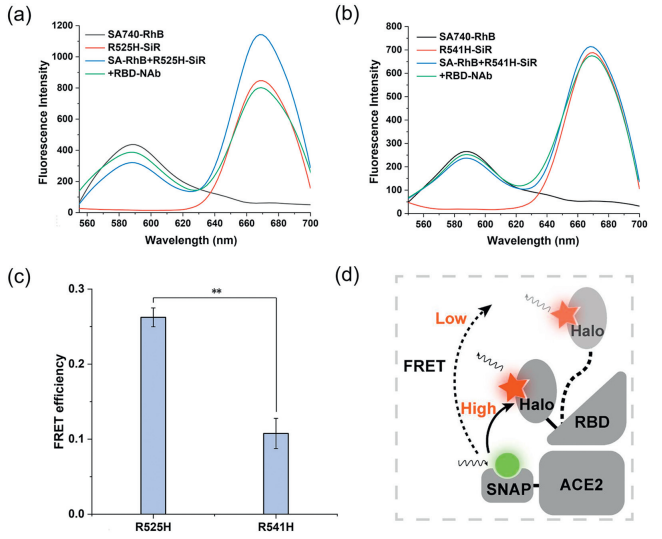

Fig. 2. Comparison of FRET efficiency between the interactions of R525H and R541H with the SA740 protein. (a, b) Emission spectra of SA740-RhB (0.2 μmol/L) interacted with R525H-SiR (0.2 μmol/L) or R541H-SiR (0.2 μmol/L), RBD neutralizing antibody (RBD-NAb) as RBD inhibitor can disrupt RAB and reduce FRET efficiency. $\lambda_{ex} = 520$ nm. (c) The FRET efficiency between the interactions of R525H and R541H with the SA740 protein. The experiments were repeated three times. Statistical analysis was by one-way ANOVA. $^{**}P < 0.05$. Quantitative data are presented as the mean ± standard deviation (SD). (d) The schematic representation of the high/low FRET effect.

Furthermore, the effects of R541H and R525H fusion proteins, before and after the truncation of s-RBD, on FRET between s-RBD and ACE2 were tested. The SNAP-RhB/Halo-SiR FRET pairs were labeled to SA740, R541H, and R525H, respectively. And the FRET between SA740&R525H and SA740&R541H was detected. As shown as in Figs. 2a and b, there was an obvious decrease in donor fluorescence intensity and an increase in acceptor fluorescence for SA740&R525H, while the changes of donor-acceptor fluorescence were weak for SA740&R541H. And a relative higher FRET efficiency of 26.2% for SA740&R525H was calculated compared to SA740&R541H with a FRET efficiency of only 10.8% (Fig. 2c). As expected, the distance between donor-acceptor fluorophores was enlarged by longer amino acid residues of R541H than R525H, and thus weakens FRET efficiency (Fig. 2d). It is demonstrated that SA740&R525H can be used to track RAB by FRET-based assay.

We then examined the impact of introducing RBD inhibitors on the FRET between SA740 and R525H to verify its potential for inhibitor screening *in vitro*. After the addition of RBD neutralizing antibody (RBD-NAb), the fluorescent intensity of SA740-RhB was increased while that of R525H-SiR was reducing (Fig. 2a), indicating that the interaction between SA740 and R525H was disrupted by RBD-NAb. Despite the relatively low FRET efficiency between SA740-RhB and R525H-SiR, its sensitivity allowed for the detection of RAB inhibitors. Moreover, after adding RBD-NAb, there was also partial restoration of FRET between R541H-SiR and SA740-RhB (Fig. 2b).

Subsequently, various known inhibitors of s-RBD and ACE2 were detected for qualitative and quantitative assessment of the effectiveness of the FRET-assisted *in vitro* screening system. The procedure involved incubating the inhibitors with s-RBD or ACE2 in a 384-well plate for 30 min, followed by the addition of the other protein to a final volume of 100 μL. Fluorescence spectra were then detected using a microplate reader (Fig. 3a). The control group consisted of only s-RBD and ACE2 proteins. Commercial ACE2-mFc and RBD-NAb as RBD inhibitors, SARS-CoV-2 wild RBD-mFc and S1 as ACE2 inhibitors were added to determine the practicality of the assay. As shown in Fig. 3b, the fluorescence intensity of the acceptor (R525H-SiR) was reduced, while the fluorescence intensity of the donor (SA740-RhB) was enhanced, and the degree of FRET effect varied for different analytes. The acceptor/donor ratiometric fluorescent intensity of the analyst was calculated as shown in Fig. 3c, where a lower acceptor/donor ratiometric fluorescent intensity represented a better inhibition effect. As expected, RBD neutraliz-

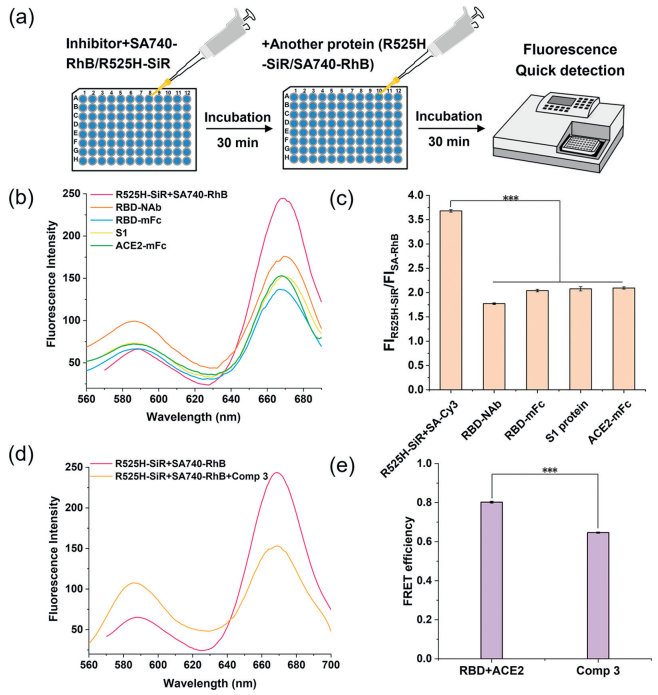

Fig. 3. FRET-based *in vitro* assay to detect various SARS-CoV-2 entry inhibitors. (a) Schematic diagram of the operating steps of FRET-based *in vitro* assay for the detection of RAB inhibitors. (b) Emission spectra of SA740-RhB (0.2 μmol/L) interacted with R525H-SiR (0.2 μmol/L) pre-incubated with RBD-NAb, RBD wild type (RBD-mFc), ACE2 wild type (ACE2-mFc), or S1. $\lambda_{ex} = 520$ nm. (c) The fluorescence intensity ratio of RBD and ACE2 protein with or without inhibitors. The experiments were repeated three times. (d) Emission spectra of SA740-RhB (0.2 μmol/L) interacted with R525H-SiR (0.2 μmol/L) pre-incubated with Comp 3. (e) The fluorescence intensity ratio of RBD and ACE2 protein with or without Comp 3. The experiments were repeated three times. Statistical analysis was by one-way ANOVA. $^{***}P < 0.005$. Quantitative data are presented as the mean ± SD.

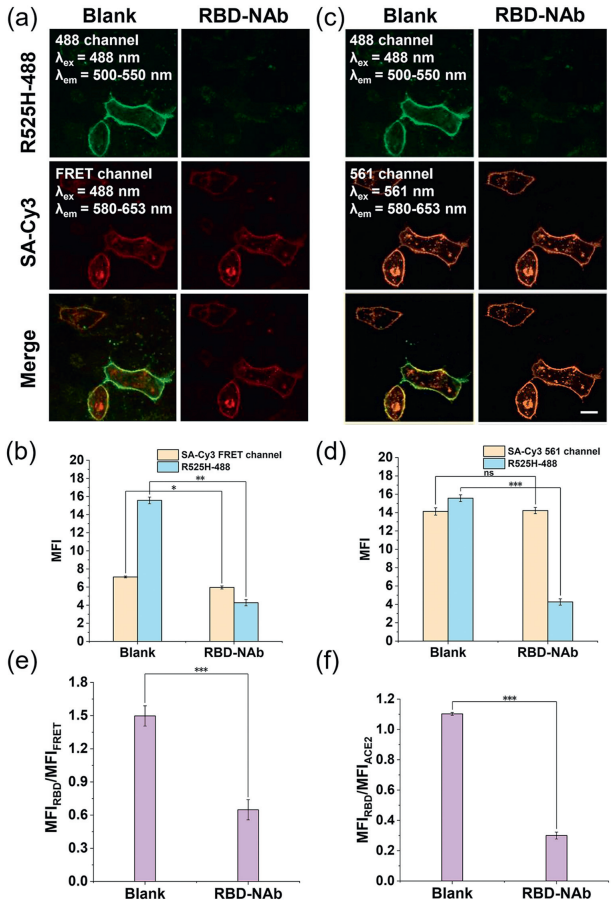

Fig. 4. FRET-based detection of RAB inhibitors in the living cells. (a) Fluorescence imaging of SA-overexpressed HeLa cells stained with SNAP-Cy3 and R525H-SiR. $\lambda_{ex} = 488$ nm, $\lambda_{em} = 500–550$ nm for 488 channel, $\lambda_{em} = 580–653$ nm for FRET channel. (b) The mean fluorescence intensity (MFI) of 488 and FRET channel without or with the addition of RBD-NAb in (a). The experiments were repeated three times. (c) Fluorescence imaging of SA-overexpressed HeLa cells stained with SNAP-Cy3 and R525H-SiR. 488 channel: $\lambda_{ex} = 488$ nm, $\lambda_{em} = 500–550$ nm. 561 channel: $\lambda_{ex} = 561$ nm, $\lambda_{em} = 580–653$ nm. Scale bar: 10 μm. (d) The mean fluorescence intensity of 488 and 561 channel without or with the addition of RBD-NAb in (c). The experiments were repeated three times. (e, f) The mean fluorescence intensity ratio of FRET assay and LCAR-RFI assay. The experiments were repeated three times. Statistical analysis was by one-way ANOVA. $^{*}P < 0.5$, $^{**}P < 0.05$, $^{***}P < 0.005$. Quantitative data are presented as the mean ± SD.

ing antibody showed the highest inhibition efficiency. And the inhibition efficiency of RBD-mFc was slightly higher than S1.

Comp 3 was identified as an RAB inhibitor in our previous work [28]. Both pseudo-virus and live-virus experiments validated the antiviral performance of this molecule. It specifically binds to s-RBD, thereby inhibiting viral entry. We evaluated the inhibitory efficiency of the small molecule compound Comp 3 using this system. Upon addition of Comp 3, a significant inhibition of FRET between R525H-SiR and SA740-RhB was observed (Figs. 3d and e), demonstrating the utility of this method for detecting small molecule inhibitors of RAB. It was demonstrated that the FRET-assisted *in vitro* screening system can rapidly, conveniently, and effectively screen inhibitors of SARS-CoV-2 entry, and qualitatively and quantitatively evaluate the efficiency of inhibitors. This system can be used for high-throughput *in vitro* screening of RAB inhibitors.

Based on the rapid and highly sensitive properties of the FRET technology, it is not only employed for drug screening in solution but also extensively used for screening various inhibitors in live cells and even *in vivo*, such as the inhibitors for DNA intercalator [32], α-synuclein [33], cancer cells [34]. Here, we further evaluated the performance of this FRET system for inhibitor detection in live cells. First, fusion protein SA (Scheme 1c) [28] was overexpressed in HeLa cells, where ACE2 was located on the outer membrane of cells, while the SNAP protein fused at the N-terminus of ACE2 was exposed to the extracellular environment. Therefore, the impermeable SNAP-dye can covalently attach to the SNAP protein. We chose Halo-488 and impermeable SNAP-Cy3 as a pair of FRET dyes (Fig. S2 in Supporting information) labeled on R525H and SA proteins, respectively, resulting in R525H-488 and SA-Cy3. SNAP-Cy3 and R525H-488 were added to HeLa cells overexpressing SA. Confocal fluorescence imaging (Fig. 4a) showed that upon excitation at 488 nm, the 488 channel (donor channel, $\lambda_{em} = 500–550$ nm) exhibited bright green fluorescence on the cell membrane, while the FRET channel ($\lambda_{em} = 580–653$ nm) displayed red fluorescence. The red and green fluorescence were colocalized on the cell surface. This indicated that R525H-488 interacted with ACE2 on the cell membrane, resulting in a certain degree of FRET. Upon addition of RBD-NAb, the fluorescence in the 488 channel on the cell membrane disappeared due to the inhibition of RAB and the departure of R525H-488. Statistical data of the mean fluorescence intensity on the cell membrane (Fig. 4b) revealed a decrease of fluorescence intensity in the FRET channel after the addition of RBD-NAb, demonstrating the inhibition of FRET. The fluorescence observed in the FRET channel at this point was due to the excitation of SNAP-Cy3 by 488 nm laser. The slight fluorescence change in the FRET channel indicated a low FRET efficiency between R525H-488 and SA-Cy3 in the living cells.

Since s-RBD interacts with ACE2 on the cell membrane, RAB inhibitors can cause the removal of s-RBD from the cell membrane, resulting in the disappearance of fluorescence. In our previous work, we developed LCAR-RFI assay to screen for SARS-CoV-2 inhibitors by directly quantifying the ratio of fluorescence from s-RBD channel and ACE2 channel on the cell membrane [28]. Here, we aimed to compare the sensitivity of screening RAB inhibitors using two methods: the ratio from MFI_{RBD}/MFI_{FRET} channel and MFI_{RBD}/MFI_{ACE2} channel, respectively. Therefore, we observed and statistically analyzed the fluorescence in the 561 channel (SNAP-Cy3 channel) of the same cell, as shown in Figs. 4c and d. Before and after adding the inhibitor, the fluorescence in the 561 channel remained bright and relatively stable. The ratio of mean fluorescence intensity between the two channels indicated that the sensitivity of screening RAB inhibitors using LCAR-RFI method is comparable to that using the FRET method (Figs. 4e and f). This is mainly because of the low FRET efficiency between R525H-488 and SA-Cy3 in live cells.

The crystal structure of the RBD-ACE2 interaction reveals a minimal distance of approximately 5.6 nm between the C-terminus of s-RBD and the N-terminus of ACE2. To enable the specific and individual attachment of fluorescently superior dyes to s-RBD and ACE2 proteins for quantitative detection, genetically coded protein tag technology is preferred. However, commonly used SNAP and Halo tags have large molecular weights, approximately 26 and 33 kDa, respectively. When fused with s-RBD and ACE2 proteins, they can increase the distance between FRET dye pairs beyond 5.6 nm. Consequently, this may result in reduced FRET efficiency between R525H and SA740. Shorter protein tags, such as peptide tags, could potentially reduce the distraction, the R525H-Dye and SA740-Dye developed in this study are suitable for screening RAB inhibitors in solution.

In summary, we developed a FRET-based method for rapidly detecting the RAB inhibitors in solution. Utilizing the site-specific and stable fluorescence labeling properties of genetically encoded Halo and SNAP protein tags on target proteins, we labeled FRET pairs of fluorescent dyes onto s-RBD and ACE2 proteins. By comparing the fluorescence spectra of three pairs of dyes labeled on proteins, we selected SNAP-RhB and Halo-SiR, which exhibit good spectral separation and possess a certain FRET effect, as the FRET pair for RAB inhibition and detection. Further analysis of two different lengths of s-RBD revealed that the truncated R525H protein can generate a better FRET effect with SA740. Therefore, based on the FRET between R525H-SiR and SA740-RhB, we found that RBD-NAb, RBD-mFc, ACE2-mFc, S1 and the small molecule inhibitor Comp 3 effectively inhibit RAB in solution, and quantitatively compare the inhibitory effects of these inhibitors. Based on its rapidity, high sensitivity, and simple operation, the FRET method holds promise as a high-throughput screening technique for inhibitors of SARS-CoV-2 entry, making it suitable for fast *in vitro* applications.

Declaration of competing interest

The authors declare that they have no known competing financial interests or personal relationships that could have appeared to influence the work reported in this paper.

CRediT authorship contribution statement

Chunyu Yan: Writing – original draft, Data curation. **Qinglong Qiao:** Synthesizing dyes. **Wei Zhou:** Data curation. **Xuelian Zhou:** Data curation. **Yonghui Chen:** Data curation. **Lu Miao:** Writing – original draft, Supervision, Funding acquisition, Conceptualization. **Zhaochao Xu:** Writing – review & editing, Supervision, Funding acquisition, Conceptualization.

Acknowledgments

This work is supported by the National Natural Science Foundation of China (Nos. 22225806, 22378385, 22078314, 22278394) and Dalian Institute of Chemical Physics (Nos. DICPI202142, DICPI202436, DMU-1&DICP UN202301).

Supplementary materials

Supplementary material associated with this article can be found, in the online version, at doi:10.1016/j.cclet.2024.110258.

References

[1] M. Hoffmann, H. Kleine-Weber, S. Schroeder, et al., Cell 181 (2020) 271–280.
[2] M.L. Yeung, J.L.L. Teng, L. Jia, et al., Cell 184 (2021) 2212–2228.
[3] B. Ju, Q. Zhang, J. Ge, et al., Nature 584 (2020) 115–119.
[4] V. Monteil, H. Kwon, P. Prado, et al., Cell 181 (2020) 905–913.
[5] A. Acharya, A.S. Pathania, K. Pandey, et al., Clin. Transl. Med. 12 (2022) e806.
[6] M. Wang, H. Yan, L. Chen, et al., PLoS One 18 (2023) e0285722.
[7] A.M. Carabelli, T.P. Peacock, L.G. Thorne, et al., Nat. Rev. Microbiol. 21 (2023) 162–177.
[8] Y. Hu, E.M. Lewandowski, H. Tan, et al., ACS Cent. Sci. 9 (2023) 1658–1669.
[9] V.P. Chavda, R. Bezbaruah, K. Deka, et al., Vaccines 10 (2022) 1926.
[10] W. Chiu, L. Verschueren, C. Van den Eynde, et al., J. Med. Virol. 94 (2022) 3101–3111.
[11] J. Liu, K. Li, L. Cheng, et al., Int. J. Infect. Dis. 103 (2021) 300–304.
[12] W. Wan, S. Zhu, S. Li, et al., ACS Infect. Dis. 7 (2020) 1409–1422.
[13] S. Yan, H. Sun, X. Bu, et al., Front. Pharmacol. 11 (2020) 548175.
[14] J. Rout, B.C. Swain, U. Tripathy, J. Biomol. Struct. Dyn. 40 (2020) 860–874.
[15] C. Nichols, J. Ng, A. Keshu, et al., Front. Pharmacol. 11 (2020) 615211.
[16] S.M. Chowdhury, S.A. Talukder, A.M. Khan, et al., J. Phys. Chem. B 124 (2020) 9785–9792.
[17] S.J.Y. Macalino, V. Gosu, S. Hong, et al., Arch. Pharm. Res. 38 (2015) 1686–1701.
[18] N. Okimoto, N. Futatsugi, H. Fuji, et al., PLoS Comput. Biol. 5 (2009) e1000528.
[19] J. Jones, R. Heim, E. Hare, et al., SLAS Discov. 5 (2000) 307–317.
[20] G. Milligan, J. Pharm. Sci. 21 (2004) 397–405.
[21] S.M. Rodems, B.D. Hamman, C. Lin, et al., Assay Drug Dev. Techn. 1 (2002) 9–19.
[22] K. Gorshkov, K. Susumu, J. Chen, et al., ACS Nano 14 (2020) 12234–12247.
[23] S. Das, T. Yin, Q. Yang, et al., P. Natl. Acad. Sci. 112 (2015) 267–276.
[24] J. Chen, W. Liu, X. Fang, et al., Chin. Chem. Lett. 33 (2022) 5042–5046.
[25] J. Li, Q. Qiao, Y. Ruan, et al., Chin. Chem. Lett. 34 (2023) 108266.
[26] W. Liu, J. Chen, Q. Qiao, et al., Chin. Chem. Lett. 33 (2022) 4943–4947.
[27] Y. Zhang, W. Zhou, N. Xu, et al., Chin. Chem. Lett. 34 (2023) 107472.
[28] L. Miao, W. Zhou, C. Yan, et al., Acta Pharm. Sin. B 12 (2022) 3739–3742.
[29] L. Miao, C. Yan, Y. Chen, et al., Cell Chem. Biol. 30 (2023) 248–260.
[30] J.B. Grimm, B.P. English, J. Chen, et al., Nat. Methods 12 (2015) 244–250.
[31] D. Si, Q. Li, Y. Bao, et al., Angew. Chem. Int. Ed. 62 (2023) e202307641.
[32] C.U. Murade, S. Chaudhuri, I. Nabti, et al., ACS Sens. 6 (2021) 2233–2240.
[33] A.R. Braun, N.N. Kochen, S.L. Yuen, et al., ASN Neuro 15 (2023) 17590914231184086.
[34] F. Xing, N. Ai, S. Huang, et al., Front. Bioeng. Biotech. 10 (2022) 839078.